

VLBL Study Group-H2B-4
AMES-HET-01-09
AS-ITP-2001-022
November 13, 2018

Probing neutrino oscillations jointly in long and very long baseline experiments

Y. F. Wang^a, K. Whisnant^b, Zhaohua Xiong^c, Jin Min Yang^c, Bing-Lin Young^b

^a *Institute of High Energy Physics, Academia Sinica, Beijing 100039, China*

^b *Department of Physics and Astronomy, Iowa State University, Ames, Iowa 50011, USA*

^c *Institute of Theoretical Physics, Academia Sinica, Beijing 100080, China*

ABSTRACT

We examine the prospects of making a joint analysis of neutrino oscillation at two baselines with neutrino superbeams. Assuming narrow band superbeams and a 100 kt water Cerenkov calorimeter, we calculate the event rates and sensitivities to the matter effect, the signs of the neutrino mass differences, the CP phase and the mixing angle θ_{13} . Taking into account all possible experimental errors under general consideration, we explored the optimum cases of narrow band beam to measure the matter effect and the CP violation effect at all baselines up to 3000 km. We then focus on two specific baselines, a long baseline of 300 km and a very long baseline of 2100 km, and analyze their joint capabilities. We found that the joint analysis can offer extra leverage to resolve some of the ambiguities that are associated with the measurement at a single baseline.

1 Introduction

Although the existing data from the Super-Kamiokande experiment [1] and various other corroborating experiments offer very strong indications of neutrino oscillations, the appearance experiment, i.e., the appearance of a flavor different from the original one, has not been convincingly performed. If neutrinos indeed oscillate, the oscillation parameters, including the leptonic CP phase, have to be determined with sufficient accuracy. Furthermore, the well-known MSW matter effect [2] has to be tested by experiments.

In spite of the various ongoing and planned neutrino oscillation experiments, additional experiments with very long baseline are needed, at least for the test of the matter effect. The recently approved superbeam facility [3], which will be available towards the later part of this decade, offers the possibility of a very long baseline (VLBL) experiment which, in conjunction with other oscillation experiments, can test thoroughly all properties of neutrino oscillations.

Among all neutrino oscillation experiments, the long baseline (LBL) experiments are particularly attractive. Since the neutrino beams are produced in an accelerator according to definite physics criteria with the detector site chosen accordingly, the experiment can be conducted in a more controlled fashion to maximize the physics output. Hence the LBL experiments will allow us to make detailed analyses of the oscillation parameters so as to provide a complete picture of the physics of neutrino oscillation. As one example of such experiments, a project called H2B is under discussion [4, 5, 6]. The neutrino super-beam for H2B would be from the newly approved high intensity 50 GeV proton synchrotron in Japan called HIPA [3] and the detector, tentatively called the Beijing Astrophysics and Neutrino Detector (BAND), is envisioned to be a 100 kt water Cerenkov calorimeter (WCC) with resistive plate chambers (RPC) [7] located in Beijing, China. The distance from HIPA to Beijing is about 2100 km. Such a very long baseline experiment would be complementary to the recently proposed J2K experiment [8] which will also use the neutrino beam from HIPA but with the Super-Kamiokande detector or its update. The distance from HIPA to Super-Kamiokande is about 300 km.

In this article, we will examine the prospects of investigating neutrino oscillations at H2B in conjunction with J2K so that the joint data at the two widely different baselines can be used in a complementary way to provide strong leverage to eliminate some of the ambiguities in the determination of oscillation parameters. The joint analysis can expand the capability of the parameter search that are not attainable by either of the experiments alone. The two baselines can work at their respective favorable energy ranges. The present work is to demonstrate this possibility. But we have not search for the best narrow beam energies for the two baselines. Assuming a narrow band meson beam and the above mentioned 100 kt WCC with RPC, we simulate the event rates for 5-year operation. The sensitivity of the event rates for the various oscillation parameters will be explored. The present work can be regarded partly as a continuation of the study of H2B Refs. [4, 5, 6] and an initial exploration of the idea of joint analyses of two detectors which we think is appropriate for oscillation physics. In Sec. 2, we discuss some of the fundamentals of neutrino oscillation and LBL experiments. In Sec. 3, we present some of our numerical results. We present the joint analyses of the data of two detectors in Sec. 4. Finally, in Sec. 5, we present our conclusions.

2 Fundamentals of neutrino oscillation and LBL experiments

If we accept all current data, there will be three distinctive mass scales provided by the five categories of experiments: long baseline, short baseline accelerator experiments such as LSND, atmospheric, solar, and reactor. If the LSND data are excluded, the three SM neutrino flavors are sufficient and no extension of the number of neutrinos beyond that of the standard model is necessary. In view of the uncertainty of the LSND data, our discussion will be restricted to the 3-flavor scenario.

The oscillation of the 3-flavor neutrinos is a system with a limited number of degrees of freedom. The system consists of 2 mass square differences (MSD), three mixing angles and one measurable CP phase. These parameters together with the matter effect determine the various survival and appearance probabilities [9]. The unitary mixing matrix in vacuum is generally parameterized as

$$U = \begin{pmatrix} c_{12}c_{13} & c_{13}s_{12} & \hat{s}_{13}^* \\ -c_{23}s_{12} - c_{12}\hat{s}_{13}s_{23} & c_{12}c_{23} - s_{12}\hat{s}_{13}s_{23} & c_{13}s_{23} \\ s_{12}s_{23} - c_{12}c_{23}\hat{s}_{13} & -c_{12}s_{23} - c_{23}s_{12}\hat{s}_{13} & c_{13}c_{23} \end{pmatrix} \quad (1)$$

where $s_{jk} = \sin(\theta_{jk})$, $c_{jk} = \cos(\theta_{jk})$, and $\hat{s}_{jk} = \sin(\theta_{jk})e^{i\delta}$, θ_{jk} defined for $j < k$ is the mixing angle of mass eigenstates ν_j and ν_k , and δ is the CP phase angle. The three mass eigenvalues are denoted as m_1 , m_2 , and m_3 . The two independent MSD are $\Delta m_{21}^2 \equiv m_2^2 - m_1^2$ and $\Delta m_{32}^2 \equiv m_3^2 - m_2^2$.

In LBL experiments the neutrino beam has to go through matter which gives rise to the well-known MSW effect [2]. A widely used model for the Earth, called the preliminary reference Earth model PREM, is given in [10] and the earth density profile can be found in [11]. Since for a VLBL experiment the matter density can vary significantly along the path of the neutrino beam, in our calculation we perform numerical integration of the Schrödinger equation for a realistic treatment of the distance dependent matter density.

The detection of a given neutrino flavor is through its accompanying charged lepton produced by the charge current interaction of the neutrino with the nucleons in the detector mass. For a neutrino energy E_ν , which is small compared to the mass of the W and Z bosons but large enough so that quasi-elastic effect is small, the charge current cross sections are given by $\sigma_{\nu N} = 0.67 \times 10^{-38} \text{cm}^2 E_\nu (\text{GeV})$ for electron and muon neutrinos, and $\sigma_{\bar{\nu} N} = 0.34 \times 10^{-38} \text{cm}^2 E_\nu (\text{GeV})$ for electron and muon anti-neutrinos. For the tau neutrino, the above expression is subject to a threshold suppression. The threshold for the production of the tau is $E_T = m_\tau + \frac{m_\tau^2}{2m_N} = 3.46 \text{ GeV}$. A fit of ν_τ to ν_μ cross section as a function of the neutrino energy in terms of the ratio of two quadratic polynomials can be found in Ref. [4]. The signal events of flavor β , i.e., the number of charged lepton of flavor β , from a neutrino beam of flavor α , to be observed at a baseline L is given by

$$N_s = \int_{E_{\min}}^{E_{\max}} \Phi(E_\nu, L) \sigma(E_\nu) P_{\alpha \rightarrow \beta}(E_\nu, L) dE_\nu, \quad (2)$$

where $\Phi(E_\nu, L)$ is the total neutrino flux spectrum including the detector size and running time period, $P_{\alpha\rightarrow\beta}(E_\nu, L)$ is the oscillation probability, $\sigma(E_\nu)$ the neutrino charge current cross section, and E_{Max} and E_{min} are the maximum and the minimum energies of the beam.

In a narrow band beam the neutrino flux is distributed below a given energy E_{peak} . The intensity is peaked at E_{peak} and decreases rapidly below E_{peak} . The wide band beam contains neutrinos with energy spread out in a significant range of energy. In our calculation we will use the realistic beam energies and profiles provided in [5, 12]. Some of the narrow band beams together with the wide beam are plotted in Fig. 1. Here $dN_{cc}/dE_\nu \equiv \Phi(E_\nu, L)\sigma(E_\nu)$ is the energy distribution of the charged-current events N_{cc} for one year operation of a 100 kt detector at $L=2100$ km.

Since in oscillation experiments, especially in the case of electron neutrino appearance, the statistics are generally not large. Therefore the error is an important factor in the physics extraction. We use the approach of Ref. [6] to estimate the possible statistical and systematic errors and to gain a sense of the goodness of the fit. For the electron counting experiments the errors and uncertainties arise from the following sources:

- (i) The statistical error in the measurement of the charge lepton of flavor β which is as usual $\sqrt{N_s + N_b}$. N_b is the number of measured background events and can be expressed as

$$N_b = f_\beta \int_{E_{\text{min}}}^{E_{\text{Max}}} \Phi(E_\nu, L)\sigma(E_\nu)dE_\nu. \quad (3)$$

- (ii) The systematic uncertainty in the calculation of the number of background events, which can be denoted as $r_\beta N_b$.
- (iii) The systematic uncertainty in the beam flux and the cross section which we denote as $g_\beta N_s$.

The total error is the quadrature of all these uncertainties. In our calculation we will take $r_\beta = 0.1$, $g_\beta = 0.05$, and $f_\beta = 0.01$.

3 Numerical results for individual baselines

Presently there are sizable errors in all the oscillation parameters. However, we envisage that at the H2B time, Δm_{32}^2 , Δm_{21}^2 , θ_{23} , and θ_{12} will be fairly accurately determined. So we will not assign any specific errors to them. We focus our investigations on the following parameters and effects: matter, MSD sign, CP violation, and θ_{13} .

3.1 Inputs

We present numerical results of a 5-year operation with a water Cerenkov detector. The detector size is assumed to be 100 kt for all baselines. Sizes other than 100 kt will be labeled whenever used.

The inputs of the mixing angles and MSD's are from solar, atmospheric and CHOOZ experiments. For definiteness we take $\sin^2(2\theta_{12}) = 0.8$ and $\sin^2(2\theta_{23}) = 1.0$. In most of our results we use $\sin^2(2\theta_{13}) = 0.05$ for illustration and effects of larger and smaller values of θ_{13} , $0.01 \leq \sin^2(2\theta_{13}) \leq 0.1$, will be investigated. The inputs of MSD Δm_{21}^2 and Δm_{32}^2 are respectively given by $\Delta m_{\text{sol}}^2 = 5 \times 10^{-5} \text{ eV}^2$ and $\Delta m_{\text{atm}}^2 = 3 \times 10^{-3} \text{ eV}^2$.

Presently the sign of the MSD's are unknown so there are 4 possibilities:

	I	II	III	IV	
Δm_{32}^2	+	+	-	-	(4)
Δm_{21}^2	+	-	+	-	

After showing the effects of all four sign combinations in the electron event numbers we will choose the sign I for illustration.

3.2 Matter effects

In Tables 1 and 2 we show the $\nu_\mu \rightarrow \nu_e$ event rates with and without matter effects for a narrow band beam with $E_{\text{peak}} = 4 \text{ GeV}$ for both baselines. It is clear that for both narrow band and wide band beams the matter effect is significant on electron event number at L=2100 km, but negligible at L=300 km. As expected, the ν_μ and ν_τ events show very little matter effect at either distance. The event rates at both baselines can be increased if different narrow band beams are used. For example, for L=2100 km the $E_{\text{peak}}=6 \text{ GeV}$ beam has twice as many electron events as the $E_{\text{peak}} = 4 \text{ GeV}$ beam.

In order to look for the optimum beam energy to measure matter effects at a given baseline, we have examined the following ratio, which is approximately the statistical significance of the matter effect and is referred to in Ref. [6] as the figure of merit,

$$R_{\text{matter}} = \frac{N_e|_{\text{with matter}} - N_e|_{\text{without matter}}}{\Delta N_e}. \quad (5)$$

Here ΔN_e is the total error of the electron event number, as discussed at the end of Sec. 2, without the matter effect. Figure 2 shows R_{matter} versus the baseline up to 3000 km for several narrow band beams for the four MSD signs combinations. We see that for L=2100 km the optimal narrow band beams for the matter effect are with peak energies in the range of $4 \sim 6 \text{ GeV}$. For example, as shown in Fig. 2 for the MSD sign I, the optimal narrow band beam has the peak energy around $E_{\text{peak}} = 4 \text{ GeV}$. For L=300 km, as expected, there is very little statistical sensitivity to the matter effect at all available energies.

Given a narrow band beam with $E_{\text{peak}} = 4 \text{ GeV}$ for L=2100 km and $E_{\text{peak}} = 0.7 \text{ GeV}$ for L=300 km, Fig. 3 shows the electron event rate versus the CP phase with or without matter effect. We see that for θ_{13} to have a fixed value or small range of uncertainties the matter effect is experimentally measurable for L=2100 km but hardly observable for L=300 km. However in the currently fully allowed range of θ_{13} , $\sin^2(2\theta_{13}) \leq 0.1$, it is

even difficult for the 2100 km baseline to distinguish the matter effect from the vacuum for the following fact: Since the electron event rate is proportional to $\sin^2(2\theta_{13})$, the electron event rates for $\sin^2(2\theta_{13}) = 0.03$ with matter effect and for $\sin^2(2\theta_{13}) = 0.1$ in the case of vacuum are the same as can be inferred from Fig. 3, it is not possible to distinguish the two. This ambiguity will be reinforced when the error is not negligible.

3.3 MSD sign effects

The sensitivity of the event rate to the sign of MSD for $\sin^2(2\theta_{13}) = 0.05$ is also shown in Tables 1 and 2 for $E_{\text{peak}} = 4$ GeV and $\delta = 0$ for both baselines, and in Fig. 4 for different energies for the two baselines as functions of the CP phase. Tables 1 and 2 show that the electron event rates are sensitive to the sign of MSD at the 2100 km baseline. It is also interesting to note that for L=300 km there is sensitivity in distinguishing signs I and IV in which both MSD are positive or negative from signs II and III in which one is positive and the other negative. This general feature is valid for other values of θ_{13} once it is determined.

In Fig. 4, in which we take $\sin^2(2\theta_{13}) = 0.05$, it shows clearly that for L=2100 km I and II are well separated from III and IV for all values of CP phase. Hence the sign of Δm_{32}^2 should be readily determined with moderate amount of electron neutrino appearance data. However, the separation of I from II depends on the value of the CP phase. In the region of small, intermediate and large value of the CP phase, the sign of Δm_{sol}^2 can be determined, but around $\delta = 130^\circ$ and $\delta = 280^\circ$ I and II are not distinguishable. The signs III and IV are almost inseparable in the whole region of δ . Hence the sign of Δm_{21}^2 will be very hard to determine if $\Delta m_{32}^2 < 0$. Then the anti-neutrino beam is needed for the determination. For L=300 km, Fig. 4 shows that it is difficult to distinguish I, II, III and IV except in very special values of the CP phase.

Unfortunately, the above result is only true if θ_{13} is already known. Similar to the situation discussed at the end of the preceding subsection, the significant uncertainty in $\sin^2(2\theta_{13})$ muddies the water. As $\sin^2(2\theta_{13})$ decreases the electron event rate will also be reduced. Therefore, it is difficult to distinguish the signs I and II of small θ_{13} with signs III and IV with a larger θ_{13} . We demonstrate the decrease of the lepton event rate with $\sin^2(2\theta_{13})$ in Fig. 4. Hence when the full range of current uncertainty of θ_{13} is include, i.e., $\sin^2(2\theta_{13}) < 0.1$, the sensitivity in distinguishing the MSD sign is lost for both baselines.

3.4 CP violation effects

Figures 3 and 4 show the electron event number versus the CP phase, modulo the matter effect. The typical total errors are also shown. The dominant error is found to be statistical, i.e., from the source (i) as described at the end of Sec. 2. We see that although the event rate varies significantly with the CP phase, as the electron event rate is not a single valued function of the CP phase, it is ambiguous to determine δ from the electron event number even for a fixed value of θ_{13} . The caveat of the uncertainty in θ_{13}

discussed in the two previous subsections made the ambiguity even more serious.

The sensitivity of the electron event rate to the CP phase depends on the beam energy as shown in Fig. 5. At some of the beam energies, e.g., 2 and 10 GeV for $L=2100$ km and 0.7 GeV for $L=300$ km, the curves are quite flat, indicating a poor sensitivity to the CP phase at such beam energies. Furthermore at almost no energies that one can determine a unique CP phase from the electron event number at either 300 km or 2100 km.

To investigate the sensitivity we define two ratios involving the two CP conserving phases: $\delta = 0^\circ$ and $\delta = 180^\circ$:

$$R_{\text{CP}}^{(0^\circ)}(\delta) \equiv \frac{N_e(\delta) - N_e(0^\circ)}{\Delta N_e(0^\circ)}, \quad (6)$$

$$R_{\text{CP}}^{(180^\circ)}(\delta) \equiv \frac{N_e(\delta) - N_e(180^\circ)}{\Delta N_e(180^\circ)}, \quad (7)$$

where $N_e(\delta)$, $N_e(0^\circ)$, and $N_e(180^\circ)$ are respectively the electron event numbers for CP phases δ , 0° and 180° , and $\Delta N_e(0^\circ)$ and $\Delta N_e(180^\circ)$ are the total error at $\delta = 0^\circ$ and $\delta = 180^\circ$. We can now define the figure of merit [6], i.e., the goodness of the fit, for the CP violation measurement as the smaller in magnitude of the two ratios:

$$F_{CP} \equiv \left[R_{\text{CP}}^{(0^\circ)}(\delta), R_{\text{CP}}^{(180^\circ)}(\delta) \right]_{\min}. \quad (8)$$

In Fig. 6 we plot $F_{CP}(\delta)$ versus the peak energy of the narrow band beam, separately for $L=2100$ and 300 km. We show six values of $\delta=0^\circ, 30^\circ, 60^\circ, 90^\circ, 120^\circ$, and 150° . The curves satisfy approximately the relation $F_{CP}(180^\circ + \delta) \approx -F_{CP}(\delta)$. Hence the curves for $\delta = 180^\circ, 210^\circ, 240^\circ, 270^\circ, 300^\circ$, and 330° can be inferred as the negatives of the above corresponding curves of δ less than 180° . The left panel is for the 100 kt detector and the right panel shows the results for a 1000 kt detector. We see that for the 100 kt detector at both baselines the effects of the finite CP phases are within 1σ from each other, including the CP conserving case. If we increase the detector size to 1000 kt, the CP violation effects can reach to the 2σ level for the beams around $E_{\text{peak}} \simeq 3\text{-}4$ GeV and $6\text{-}7$ GeV for $\delta = 60^\circ\text{-}120^\circ$ and $240^\circ\text{-}300^\circ$ at $L=2100$ km, and around $E_{\text{peak}} \simeq 0.7$ GeV for the similar δ ranges at $L=300$ km.

3.5 Effects of the uncertainty of $\sin^2(2\theta_{13})$

In all the above results we have used $\sin^2(2\theta_{13}) = 0.05$. Since $\nu_\mu \rightarrow \nu_e$ is proportional to $\sin^2(2\theta_{13})$, the latter is a sensitive parameter for the electron event number. Accordingly, the counting experiment of the electron event number may provide a good measurement for the value of $\sin^2(2\theta_{13})$.

In Fig. 7 we present the electron event number versus the CP phase for different $\sin^2(2\theta_{13})$ values. The error bars indicate the size of the estimated total errors. From the total errors, we see how precisely the $\sin^2(2\theta_{13})$ value can be measured. For example, for $L=2100$ km the curve of $\sin^2(2\theta_{13}) = 0.08(0.06)$ lies about 1.5σ (3σ) away from that

of $\sin^2(2\theta_{13}) = 0.1$. Then it is difficult to distinguish 0.1 from 0.08 all along the curves. Furthermore without knowing the CP phase, it may be difficult to distinguishing 0.1 at one CP phase to 0.6 at another CP phase. This ambiguity is even more serious for $L=300$ km because there is more variation of the event number as a function of the CP phase.

4 Joint analysis of baselines 2100 and 300 km

We imagine that major efforts of the very long baseline experiments such as H2B are the confirmation of the matter effect, the determination of the MSD signs, the CP phase, and θ_{13} . However, there exist difficulties in finding unique solutions for them, given the measured electron event rate, as demonstrated in the preceding section. We have discussed repeatedly in the previous section the ambiguities caused by the current wide range of uncertainty in θ_{13} . There are other ambiguities which are caused by the multi-valueness of the oscillation probability as a function of the oscillation parameters and the possibility of overlapping parameter regions. To illustrate the latter ambiguity let us consider Fig. 4. For the simplicity of argument, let us ignore any possible errors. Suppose a measurement of the electron event rate is 60 at 300 km baseline for a narrow band beam with peak energy 0.7 GeV. Then the CP phase can be either around 0° or 150° for $\sin^2(2\theta_{13}) = 0.05$. Similarly, suppose a measurement at the 2100 km baseline gives, say, the electron event rate is 40 at 4 GeV. Then CP phase can be either 150° or 300° for $\sin^2(2\theta_{13}) = 0.05$. Further, since the value of $\sin^2(2\theta_{13})$ is unknown, we in fact obtain a curve in the $\delta - \sin^2(2\theta_{13})$ plane for a given electron event number, as shown in Fig. 8. Hence the measurement from only one experiment, either at $L=300$ km or at $L=2100$ km, is not enough to determine CP phase or the value of $\sin^2(2\theta_{13})$.

To illustrate the advantage of the joint analysis of two widely different baselines, we plot in Fig. 8 $\sin^2(2\theta_{13})$ vs δ for measured electron event rates for both 300 km and 2100 km baselines at respectively 60 and 40 events for the MSD sign I. In the absence of any errors, the intersect of the curves gives unique values of both $\sin^2(2\theta_{13})$ and δ . In reality the situation will be more complicated due to the presence of errors of the measurements, and hence the intersect of the two curves will cover a sizable area of the $\sin^2(2\theta_{13})$ vs δ plane. However, this example shows the possibility of extra leverages one can gain with two different baselines.

In this section we present some of our analyses of such joint measurements, taking the advantage of superbeams like HIPA, which can offer multiple narrow band beams of different energies. We use different energies at the two baselines. We will plot 2100 km baseline vs 300 km baseline by simultaneously looking at two different parameters.

4.1 $\sin^2(2\theta_{13})$ and the CP phase δ

In Fig. 9 we show electron event number at $L=2100$ km versus those at $L=300$ km for fix MSD sign I. Each curve has a fixed value of $\sin^2(2\theta_{13})$ with the CP phase δ varies in the full possible range from 0° to 360° . The $\delta = 0^\circ$ point is marked by a solid dot

and the $\delta = 180^\circ$ point by a cross. The direction of increasing δ is indicated by the arrow on the curve. The curves are generally ellipses and the eccentricity of the ellipse is determined by the specific beam energies of the two baselines.

We fix 0.7 GeV for the 300 km baseline and allow the energy at 2100 km to change. The upper diagram of Fig. 9 is at 4 GeV for 2100 km. When $\sin^2(2\theta_{13})$ increases the ellipse moves towards the upper right, i.e., increasing the electron event rate for both baselines. This is expected from the fact that the oscillation probability $\nu_\mu \rightarrow \nu_e$ is proportional to $\sin^2(2\theta_{13})$. Since the ellipses of neighboring values of $\sin^2(2\theta_{13})$ overlap significantly, the value of δ and $\sin^2(2\theta_{13})$ can not be determined uniquely, reflecting again the ambiguities discussed in the preceding section. However there are energies at which the overlap of the ellipses is minimized. The lower diagram of Fig. 9 shows that the ellipses of constant θ_{13} are collapsed into lines when the beam energy of the 2100 km baseline is 6.3 GeV. So in principle the joint measurement allow us to narrow down the allowed range of $\sin^2(2\theta_{13})$. For the lines each measurement still allows two values of δ . But the two values of δ which fall on top of one another on the line segment will be separated when the line becomes an ellipse. So measurements at both 6.3 and 4 GeV will offer a better possibility to determined the values of $\sin^2(2\theta_{13})$ and δ simultaneously.

In Table 3 we present, for the case of MSD sign I, some E_{peak} values in GeV of narrow band beams where the ellipses of Ne(300) versus Ne(2100) as the CP Phase varies from 0° to 360° collapse into lines. At these energies the curves for MSD sign II are ellipses of high eccentricities which approximate lines. For MSD signs III and IV, and in the absence of matter effect the curves are ellipse of very high eccentricities. For these energies the combined measurements of electron event at L=2100 km and L=300 km can provide better measurement for the $\sin^2(2\theta_{13})$.

4.2 MSD sign and the CP phase δ

In Fig. 10 we present similar results, but for different MSD signs with fixed $\sin^2(2\theta_{13}) = 0.05$. The results without the matter effect are also plotted, with the dotted curves denoting MSD sign II or III and dashed ones I or IV. In the absence of the matter effect MSD signs I and IV give the same results, so do the MSD signs II and III, as already shown in Tables 1 and 2. For the almost overlapped curves of MSD sign III and IV with matter effects, the solid ones denote III and dotted ones IV.

It is clear from Fig. 10 that in the lower diagram, i.e., 6.3 GeV for the 2100 km baseline, it is quite easy to differentiate MSD signs I and II from III and IV, and from the case without the matter effect. To make better measurements it is again better to take measurements with the line together with the ellipse.

5 Conclusion

In the above study of the event rates and the sensitivity to various oscillation parameters investigated, we found:

- (a) At the distance $L=2100$ km, a narrow band beam with peak energy of about 6 GeV is optimum for measuring CP violation effects and about 5 GeV for measuring matter effects.
- (b) To measure the CP violation effect at a shorter distance such as $L=300$ km, a narrow band beam with lower peak energy (~ 0.7 GeV) is preferable. But the matter effect is hardly observable at such a shorter baseline.
- (c) The two baselines, 300 km and 2100 km, are complementary to each other. Through the joint analysis of the two baselines, some of the ambiguities associated with the measurement at either baselines may be resolved.

With the optimum narrow band beam, a 5-year operation of a 100 kt water Cerenkov detector at a very long distance such as $L=2100$ km has the following physics prospects:

- (1) The matter effects can be observed.
- (2) The sign of Δm_{32}^2 may be determined.
- (3) The sign of Δm_{21}^2 may be determined only in favorable situations.
- (4) Evidence exceeding $2\text{-}\sigma$ of a CP violating phase may be seen in favorable cases for a detector size of 1000 kt or with a much longer running time.
- (5) Combined with the analyses of $L=300$ km, the parameter $\sin^2(2\theta_{13})$ may be measured and the matter effects are more clearly determined.

In this article we have focused on the $\nu_\mu \rightarrow \nu_e$ exclusively. The investigation of the τ appearance and the inclusion of the $\bar{\nu}_\mu$ beam option in the analysis, which is needed in the cases of MSD signs III and IV, i.e., $\Delta m_{32}^2 < 0$, will be taken for a future investigation. There we will also make a more complete search for the best energies of the two baselines for the various parameters.

We finally note that the statistics are generally low in all the cases discussed. Running with higher energy narrow band beam will increase the statistics. However, that may be disfavored by the figure of merit (signal to error ratio). Another way to increase the statistics is to increase the detector mass. It has been pointed out, however, that there is a saturation problem [13] caused by the systematic errors which are of the form of the errors of types (ii) and (iii) as discussed at the end of Sec. 2. These errors increase linearly as the number of events rather than the square root of the number of events as is in the case of the statistical error. Hence, when the mass of the detector is increased so that the number of events becomes sufficiently large, the systematical error becomes dominant. After that, further increase of the detector size may no longer be beneficial. In Fig. 11 we show the ratio of ΔN_e to N_e as a function of the detector mass. We see that according to our general error estimate the best ΔN_e to N_e ratio can be attained is 6%. When the detector reaches 1000 kt the benefit of further increasing the detector size is no long significant.

Acknowledgment

We thank K. Hagiwara and N. Okamura for discussions. We also thank our colleagues of the H2B collaboration [4] for support. This work is supported in part by DOE Grant No. DE-FG02-G4ER40817.

References

- [1] Y. Fukuda *et al.*, Phys. Rev. Lett. B 81 (1998) 1562.
- [2] L. Wolfenstein, Phys. Rev. **D17**, 2367 (1978); **D20**, 2634 (1979); S.P. Mikheyev and A. Yu. Smirnov, Yad. Fiz. **42**, 1441 (1986); Nov. Cim. **9C**, 17 (1986).
- [3] HIPA: A multipurpose high intensity proton synchrotron at both 50 GeV and 3 GeV to be constructed at the Jaeri Tokai Campus, Japan has been approved in December, 2000 by the Japanese funding agency. The long baseline neutrino oscillation experiment is one of projects of the particle physics program of the facility. More about HIPA can be found at the website: "http://jkj.tokai.jaeri.go.jp".
- [4] H. Chen, et al., *Study Report: H2B, Prospect of a very Long Baseline Neutrino Oscillation Experiment, HIPA to Beijing*, hep-ph/0104266.
- [5] M. Aoki, K. Hagiwara, U. Hayato, T. Kobayashi T. Nakaya, K. Nishikawa and N. Okamura, hep-ph/0104220.
- [6] Y.-F. Wang, K. Whisnant and Bing-Lin Young, hep-ph/0109053, to appear in Phys. Rev. D.
- [7] Y.-F. Wang, hep-ex/0010081, talk given at "NEW Initiatives in Lepton Flavor Violation and Neutrino Oscillations with Very Long Intense Muon Neutrino Sources", Oct. 2-6, 2000, Hawaii, USA.
- [8] J2K: Y. Ito, et. al., *Letter of Intent: A Long Baseline Neutrino Oscillation Experiment the JHF 50 GeV Proton-Synchrotron and the Super-Kamiokande Detector*, JHF Neutrino Working Group, Feb. 3, 2000. The JHF is renamed as HIPA.
- [9] For a detail discussion of the parameter counting, see V. Barger, Y.-B. Dai, K. Whisnant, Bing-Lin Young, Phys. Rev. **D59**, 113010 (1999).
- [10] A. M. Dziewonski and D. L. Anderson, Phys. Earth Planet. Inter., 25, 297 (1981).
- [11] F. D. Staacy, *Physics of the Earth* (John Wiley & Sons, 1977); D. J. Anderson, *Theory of the Earth* (Blackwell Scientific Pub., 1989.)
- [12] The HIPA superbeam profiles are available at <http://neutrino.kek.jp/JHF-VLBL>.
- [13] V. Barger, S. Geer, R. Raja, and K. Whisnant, Phys. Rev. **D63**, 113011 (2001) (arXiv: hep-ph/0012017).

Table 1: Event rates of 5-year operation with (without) matter effects for different MSD sign choices for a narrow band beam of $E_{\text{peak}} = 4$ GeV. The CP-phase is taken to be zero.

		electron #	muon #	tau #
L=2100 km	I	34 (10)	430 (435)	10 (11)
	II	46 (16)	405 (415)	11 (11)
	III	3 (16)	413 (415)	12 (11)
	IV	3 (10)	427 (435)	11 (11)
L=300 km	I	159 (157)	39408 (39407)	72 (72)
	II	119 (116)	39535 (39535)	71 (71)
	III	114 (116)	39535 (39535)	71 (71)
	IV	154 (157)	39408 (39407)	72 (72)

Table 2: Same as Table 1, but for a wide band beam.

		electron #	muon #	tau #
L=2100 km	I	151 (96)	2313 (2311)	448 (453)
	II	151 (90)	2326 (2333)	443 (449)
	III	39 (90)	2335 (2333)	454 (449)
	IV	49 (96)	2308 (2311)	458 (453)
L=300 km	I	453 (443)	271536 (271535)	731 (731)
	II	359 (348)	271842 (271842)	718 (718)
	III	337 (348)	271843 (271842)	718 (718)
	IV	431 (443)	271535 (271535)	731 (731)

Table 3: Some E_{peak} values (GeV) of narrow band beams where the ellipses of Ne(300) versus Ne(2100) as CP Phase varies from 0° to 360° collapse into line segments. The MSD sign is assumed to be case I.

$E_{\text{peak}}(300)$	$E_{\text{peak}}(2100)$				
0.70	0.750	1.215	1.85	2.30	6.30
0.80	0.820	1.10	1.98	2.25	7.60
0.85	0.820	1.20	2.05	2.19	8.30

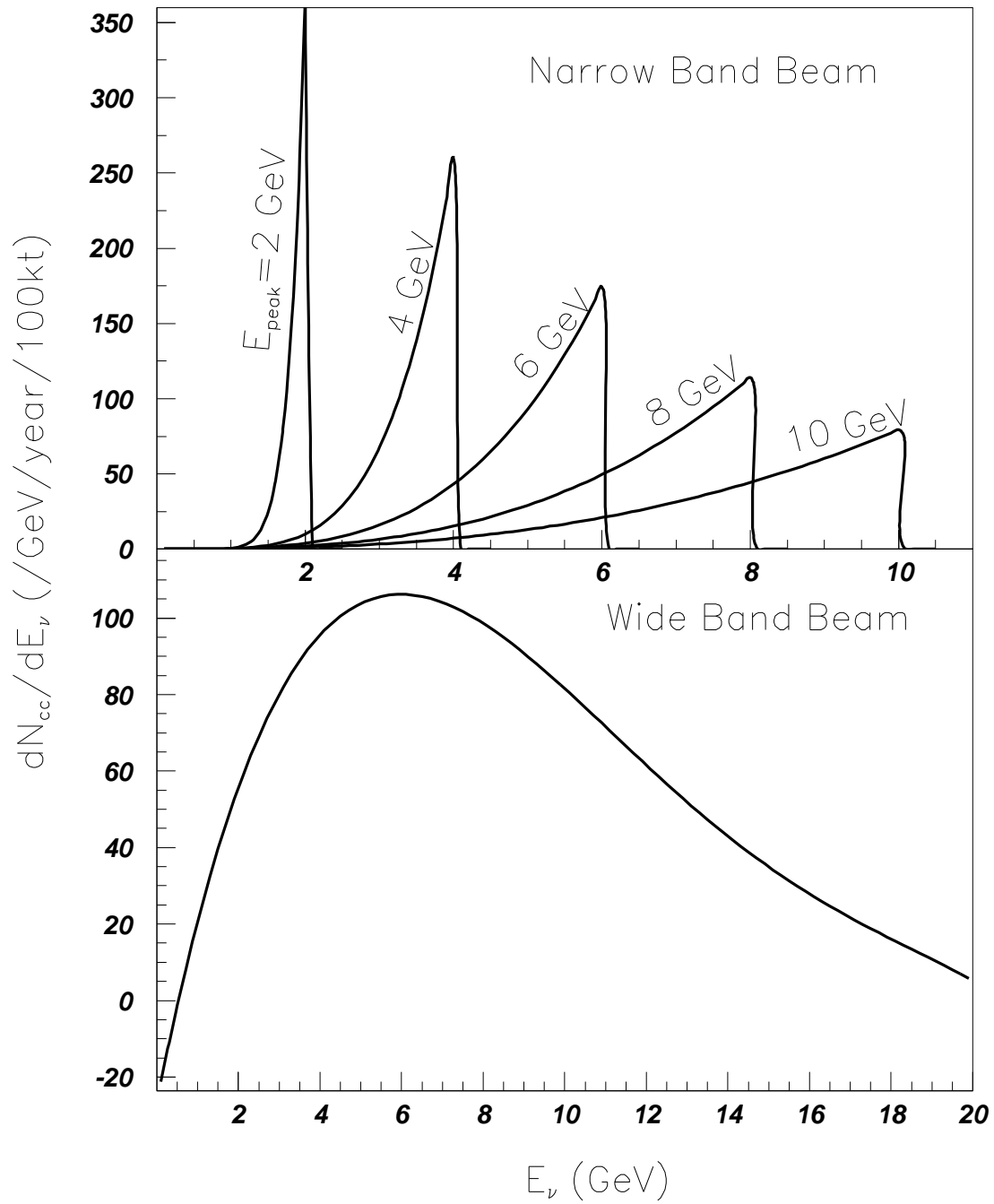


Figure 1: The energy E_ν distribution of charged-current events N_{cc} for one year operation of a 100 kt detector.

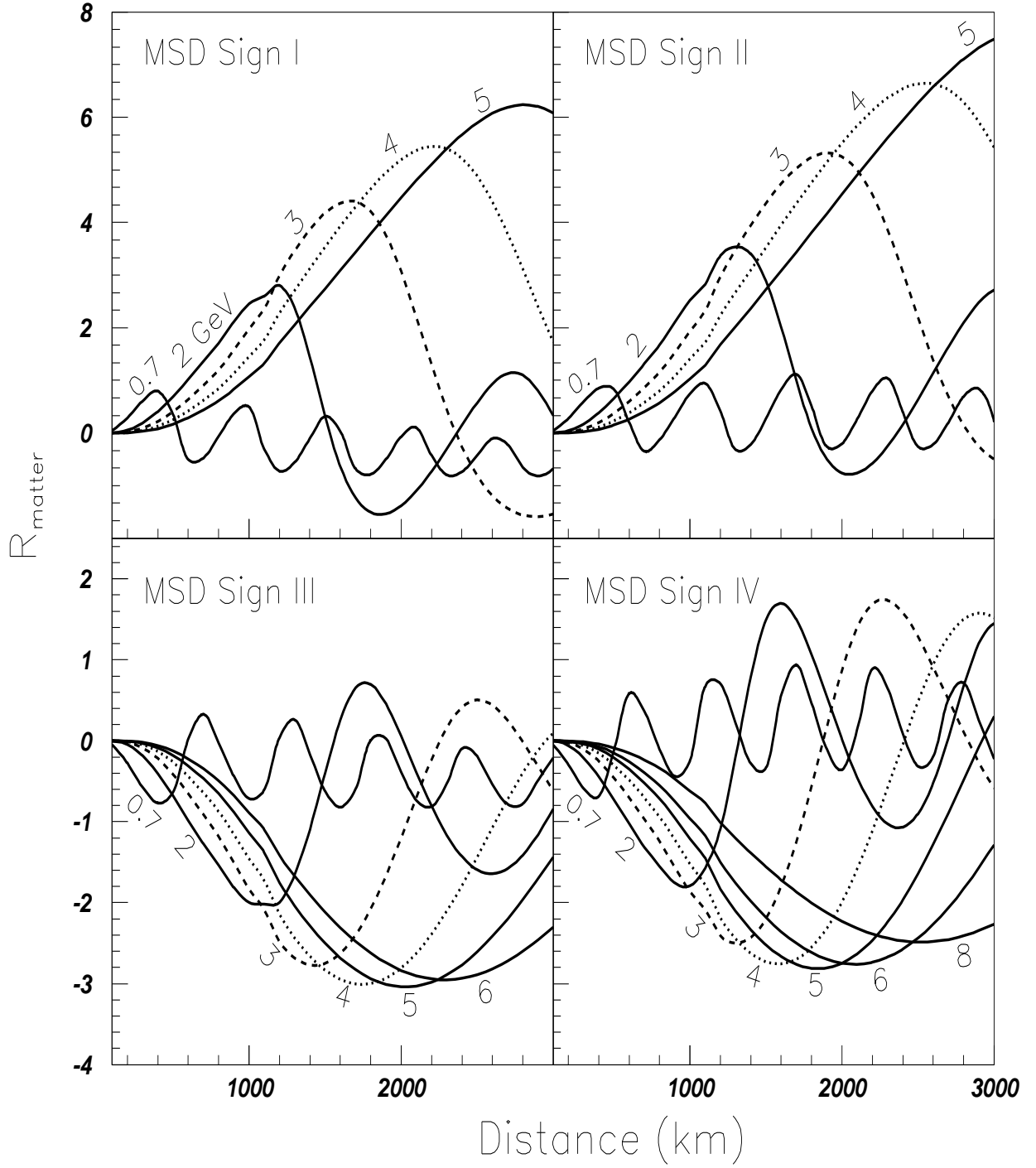


Figure 2: R_{matter} (Eq. (5)) versus the baseline for several narrow band beams. The CP phase δ is taken to be zero and $\sin^2(2\theta_{13}) = 0.05$.

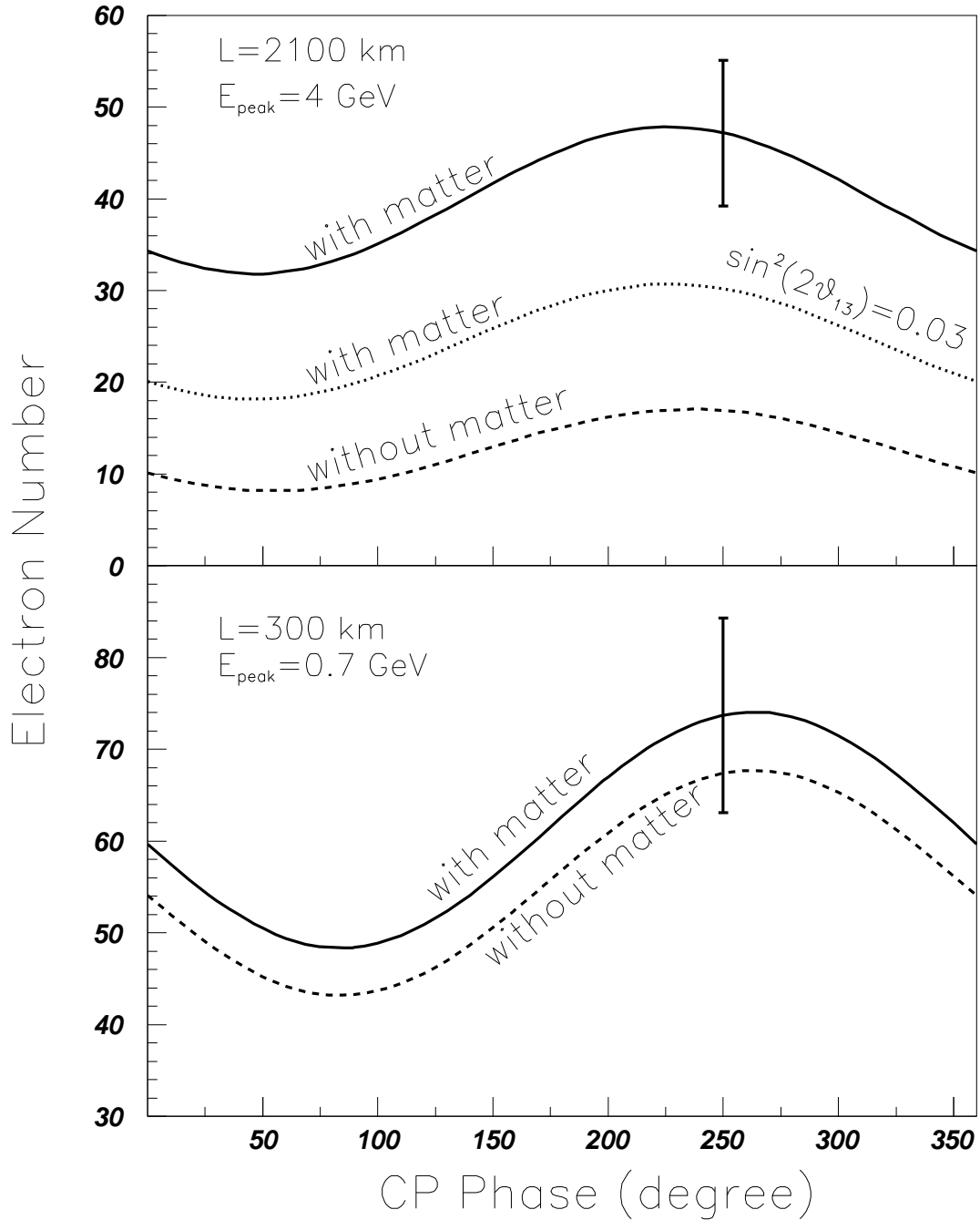


Figure 3: The electron event number versus the CP phase with and without the matter effect. $\sin^2(2\theta_{13})$ is assumed to be 0.05 except for the dotted curve which is for $\sin^2(2\theta_{13}) = 0.03$ to show the effect of varying θ_{13} . Representative total errors are also shown. The MSD sign is assumed to be I.

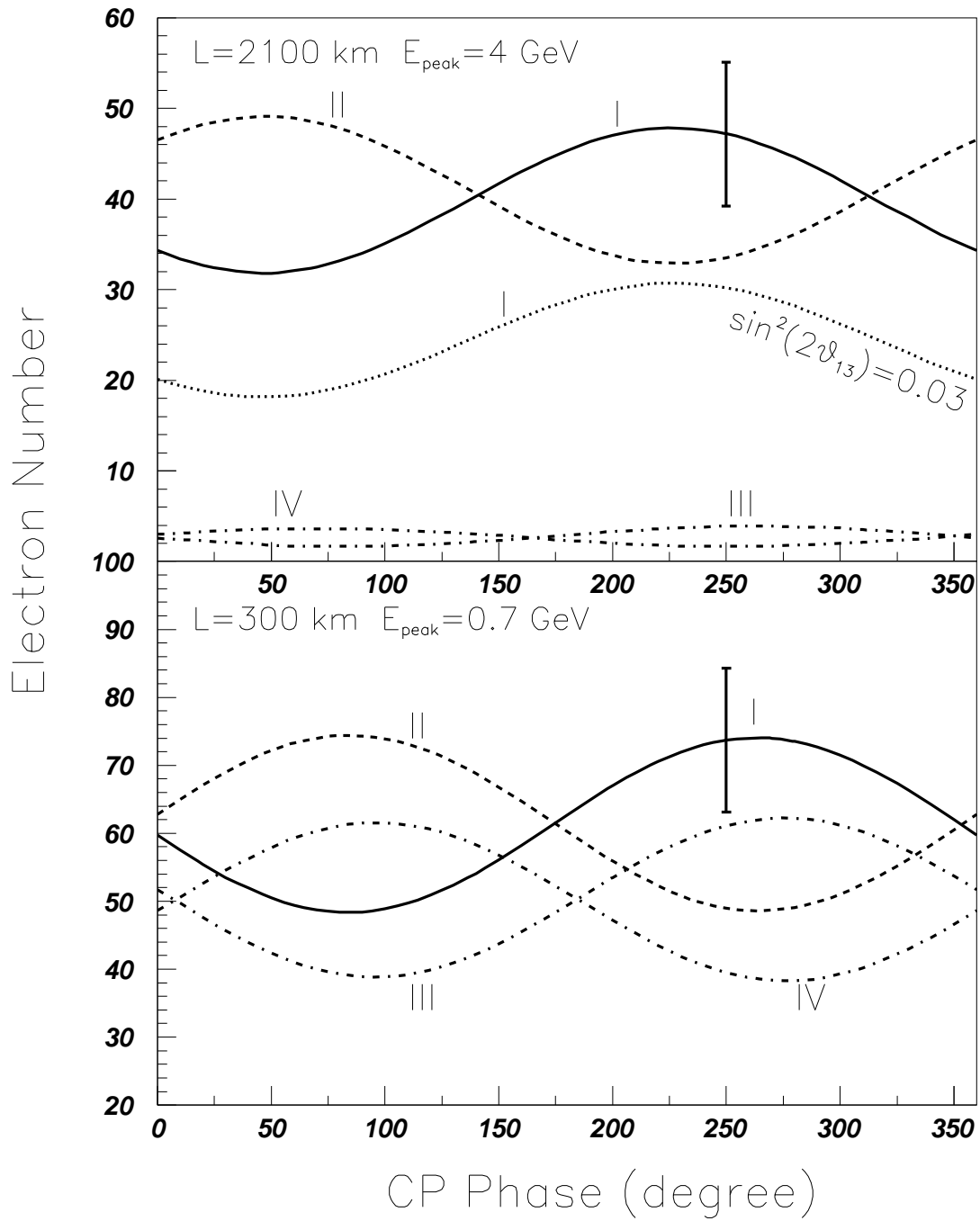


Figure 4: Same as Fig. 3, but for different MSD signs with matter effect.

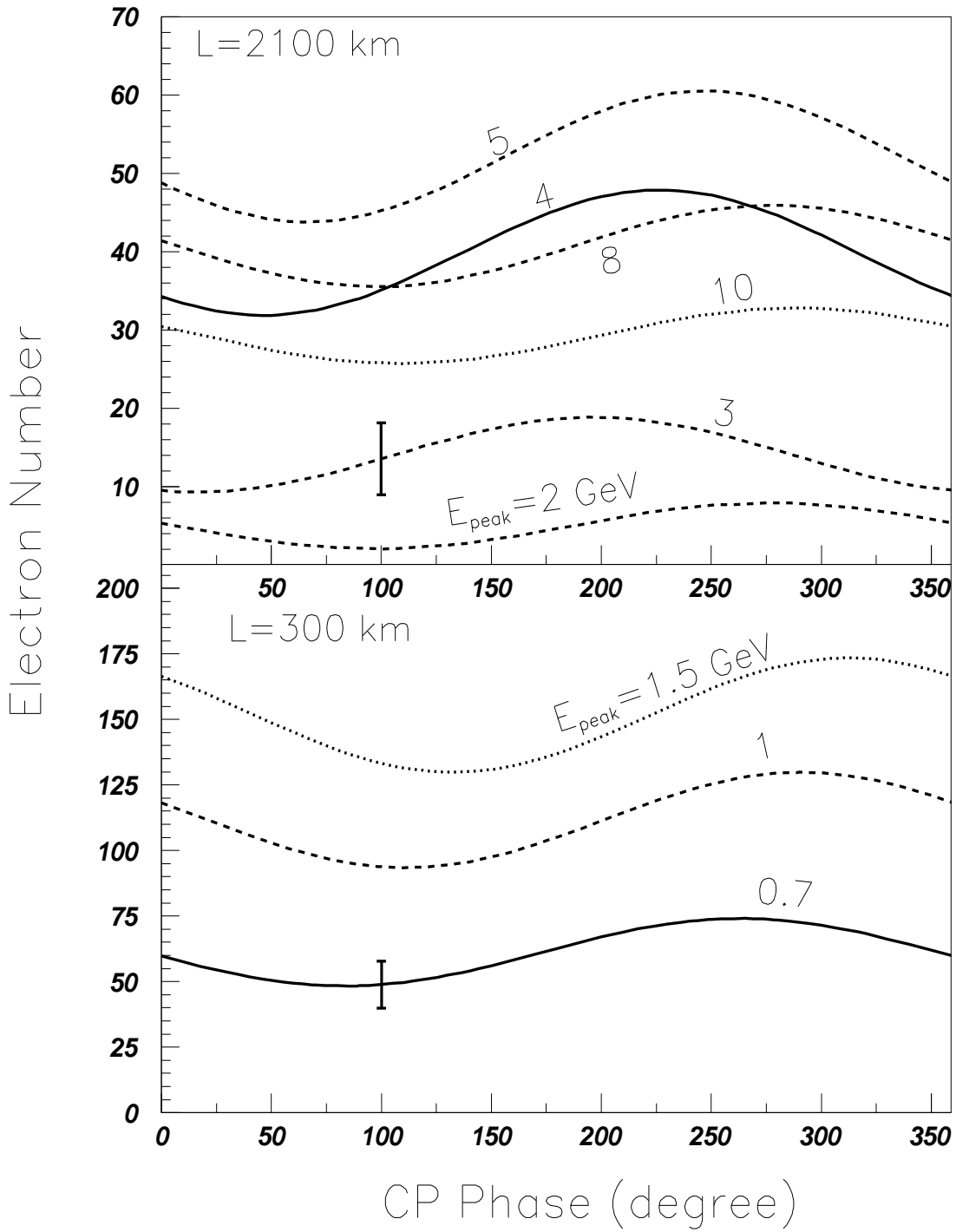


Figure 5: The electron event rate versus the CP phase for different narrow band beams. The MSD sign is assumed to be I.

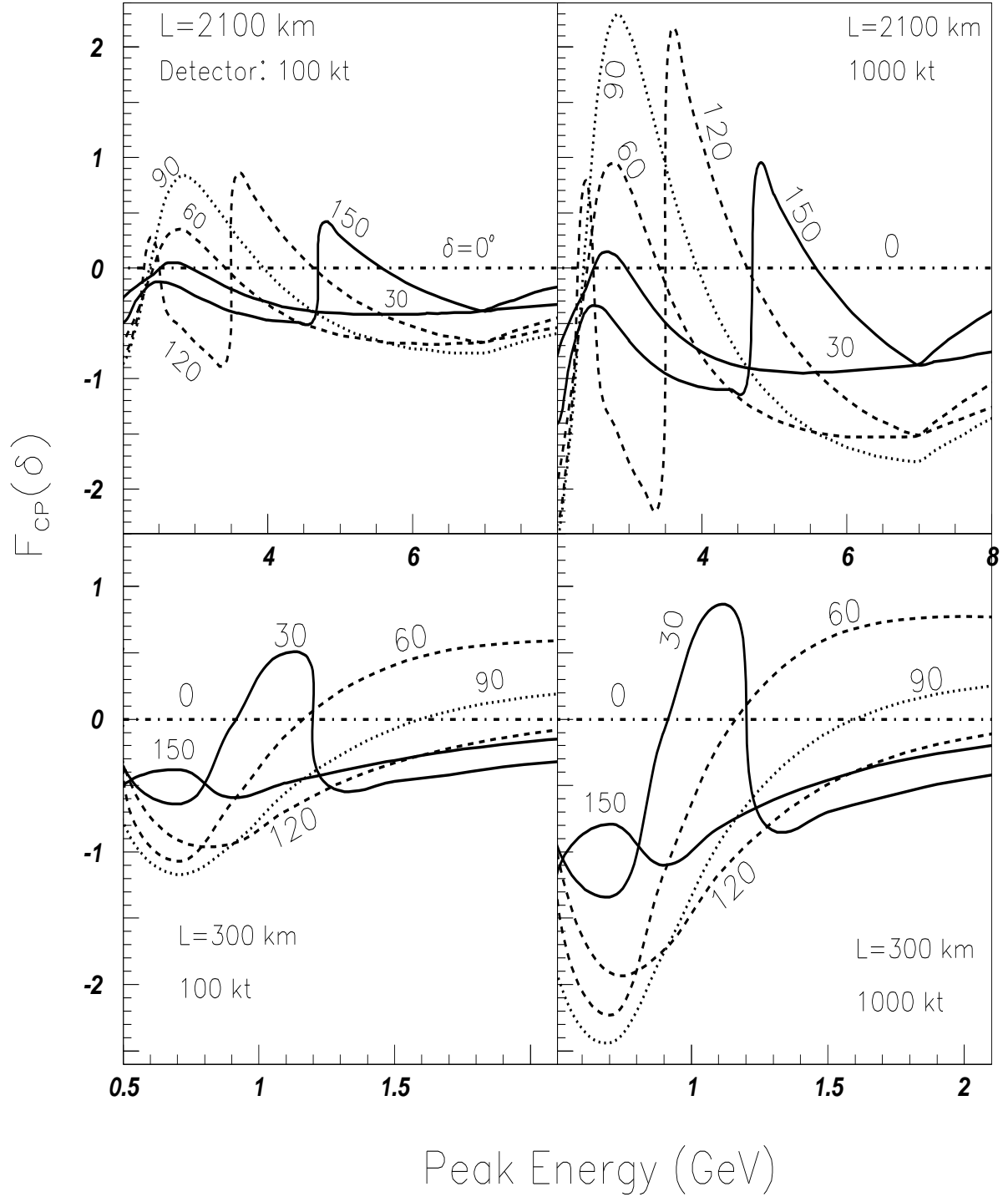


Figure 6: $F_{CP}(\delta)$ (Eq. (8)) versus the peak energy of the narrow band beams. The MSD sign is assumed to be I. With the approximate relation, $F_{CP}(180^\circ + \delta) = -F_{CP}(\delta)$, the curves for $\delta = 180^\circ, 210^\circ, 240^\circ, 270^\circ, 300^\circ,$ and 330° can be inferred.

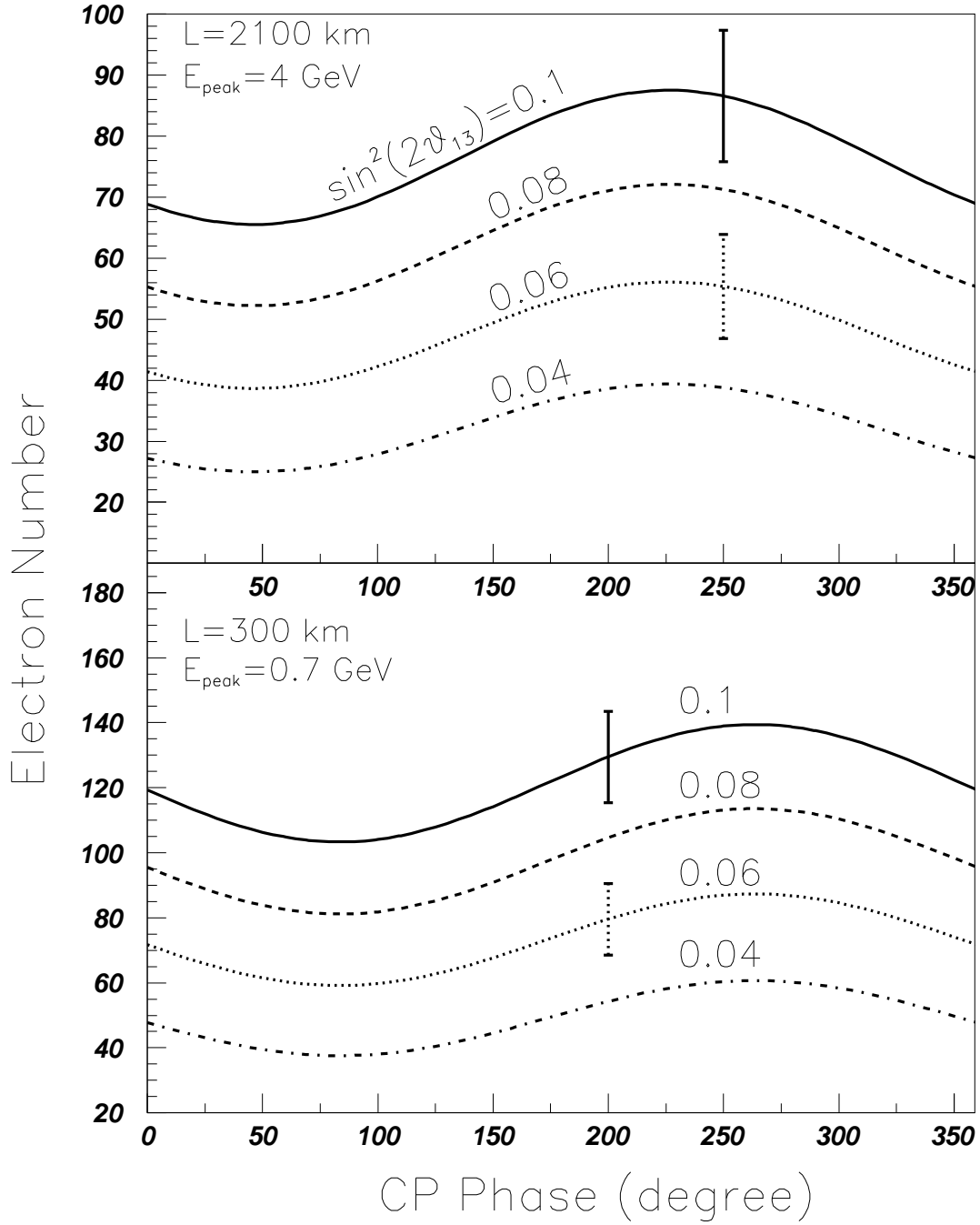


Figure 7: The electron event number versus the CP phase for different $\sin^2(2\theta_{13})$ values. The MSD sign is assumed to be I. Total errors at some points are also shown.

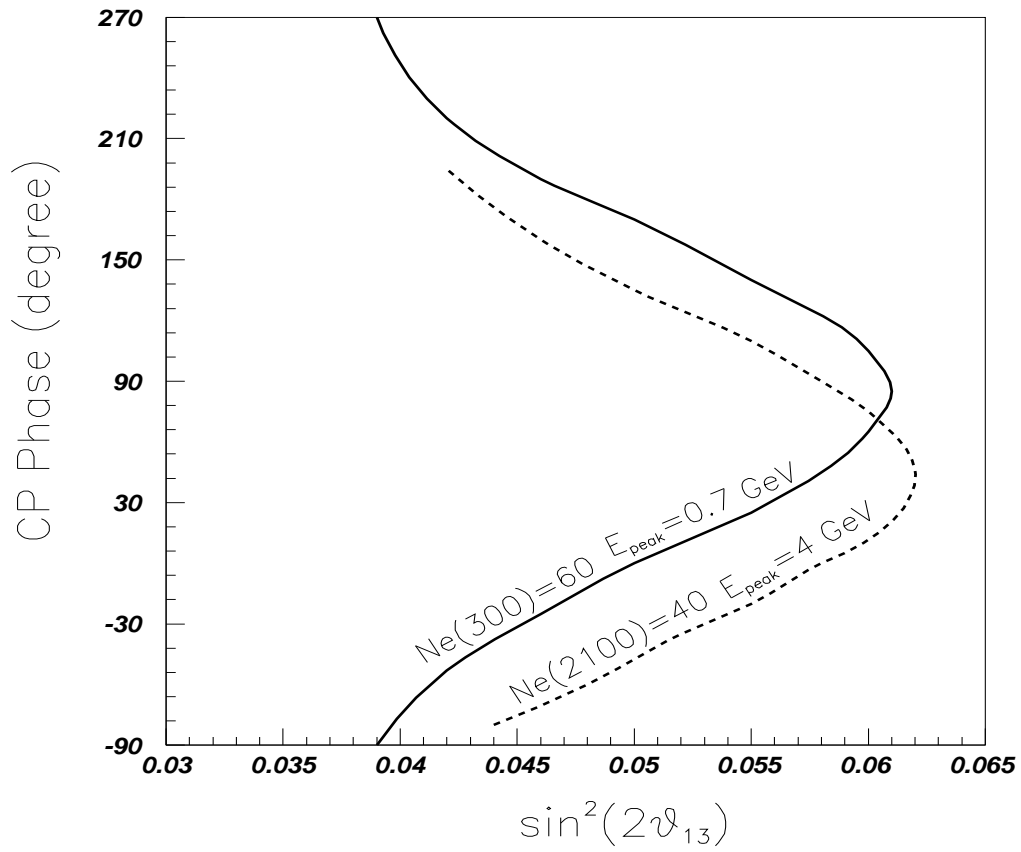


Figure 8: The CP phase versus $\sin^2(2\theta_{13})$ for a given electron event number N_e . The solid (dashed) curve is for $N_e = 60$ (40) at $L=300$ km (2100 km) with a narrow band beam $E_{\text{peak}} = 0.7$ GeV (4 GeV). The MSD sign is assumed to be I.

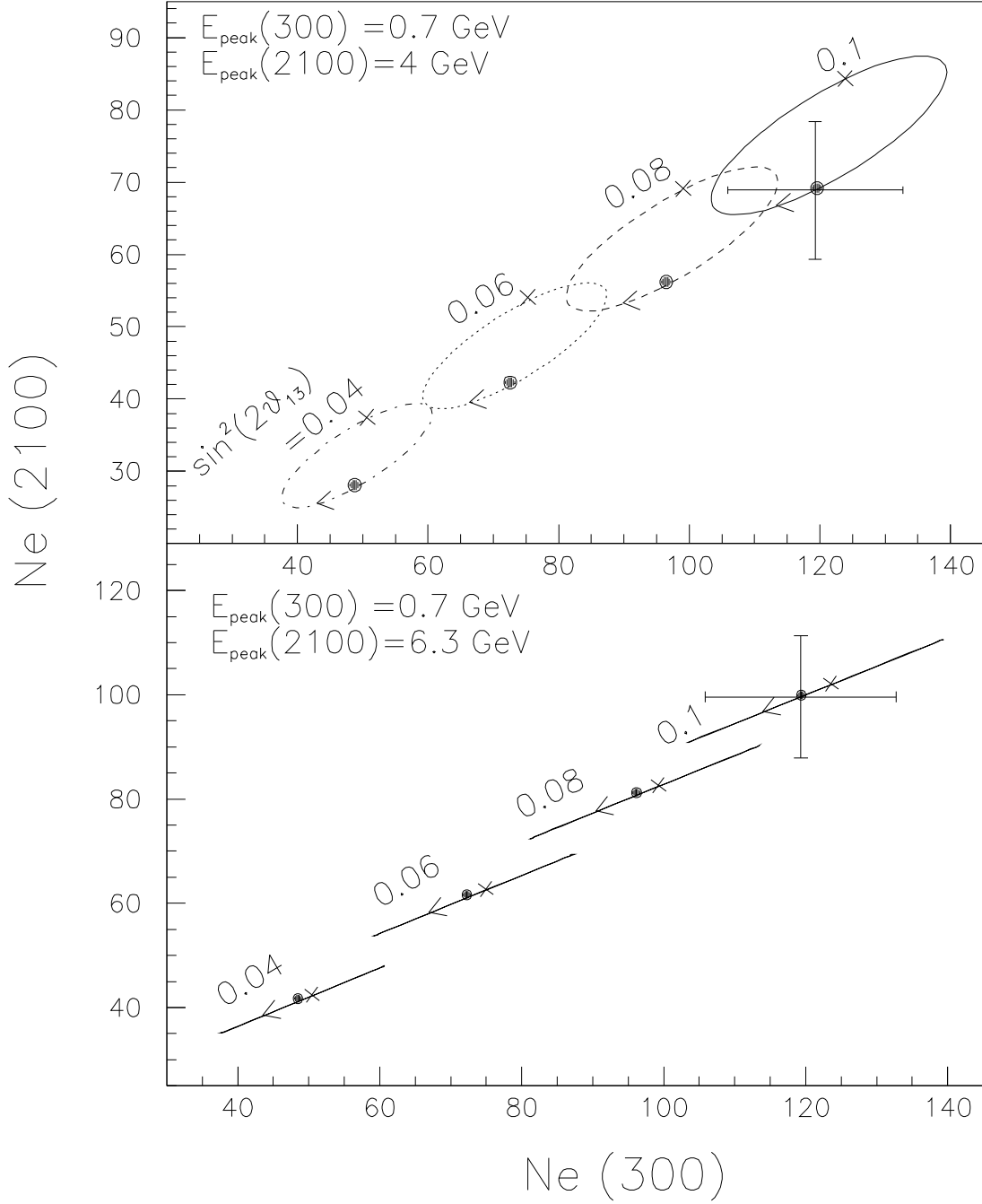


Figure 9: Electron event number at $L=2100 \text{ km}$ versus $L=300 \text{ km}$ for different $\sin^2(2\theta_{13})$ values. The CP phase δ increases from 0° (solid bullets) to 180° (crosses) then to 360° according to the direction indicated by the arrows. The MSD is assumed to have the sign I. In the lower digram for $E_{\text{peak}}(300) = 0.7 \text{ GeV}$ and $E_{\text{peak}}(2100) = 6.3 \text{ GeV}$, the ellipses collapse into line segments. The typical total errors are also shown.

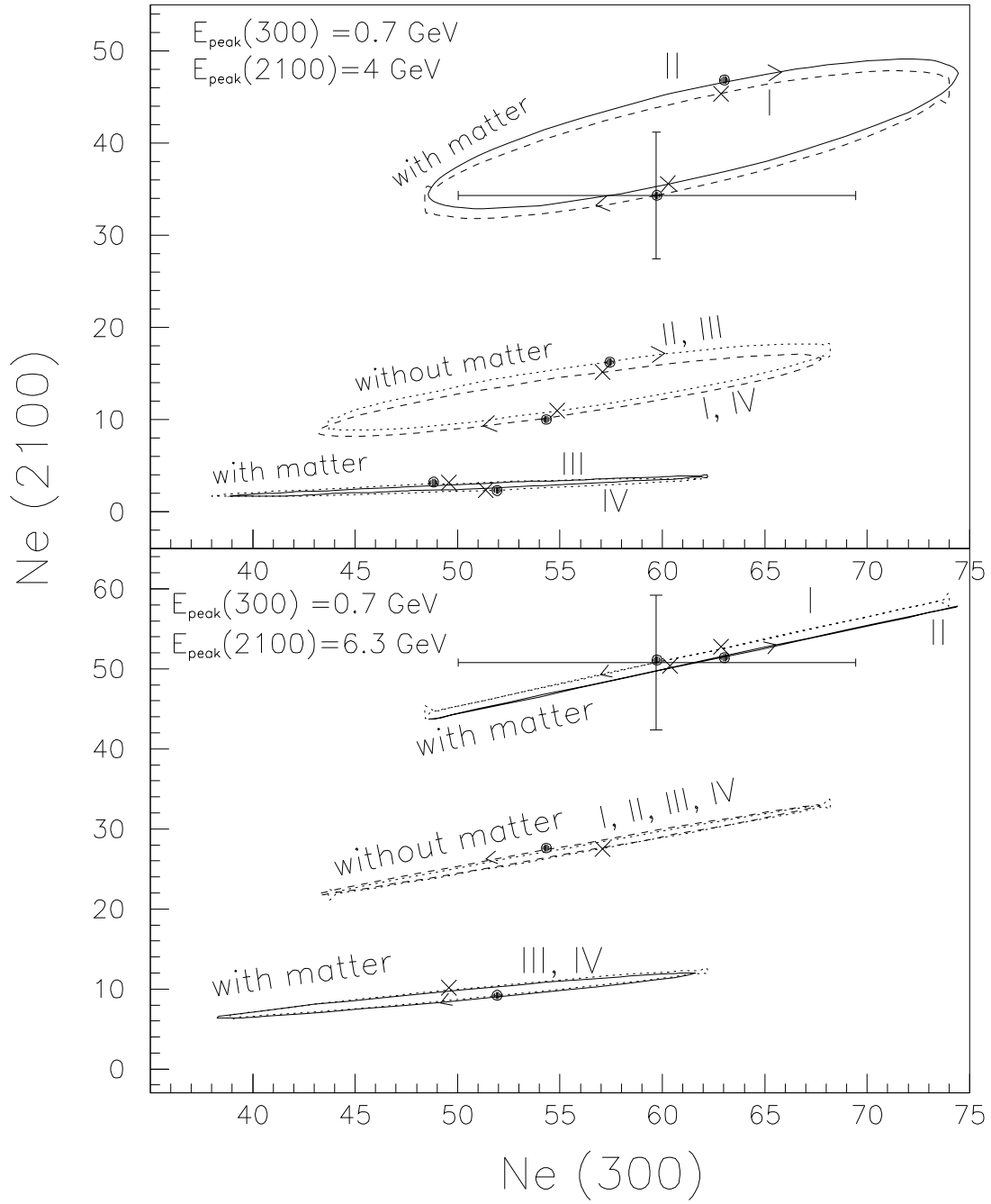


Figure 10: Similar to Fig. 9 for different MSD signs with fixed $\sin^2(2\theta_{13}) = 0.05$. The results without matter effects are also plotted.

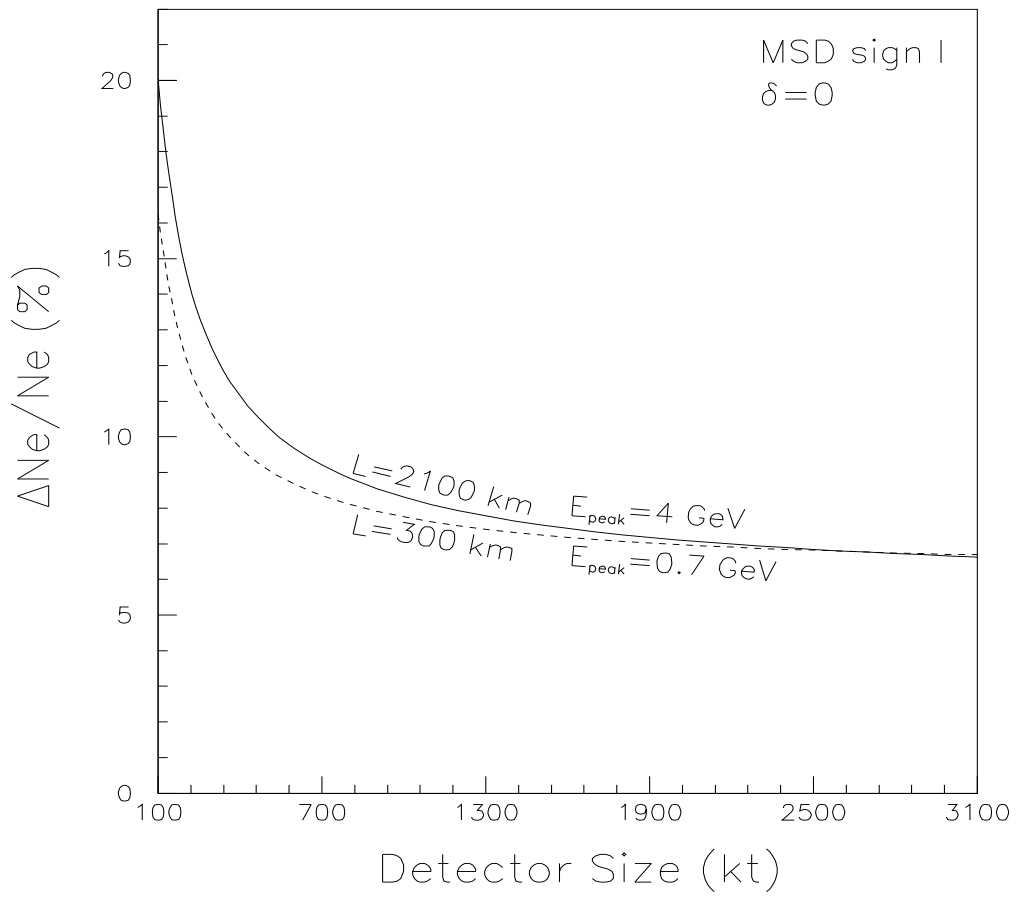


Figure 11: The relative error $\Delta N_e/N_e$ versus the detector size for a 4 GeV narrow band beam.